

P-wave excited B_c^{**} meson photoproduction at the LHeC

He Kai, Bi Huan-Yu*, Zhang Ren-You, Li Xiao-Zhou and Ma Wen-Gan

State Key Laboratory of Particle Detection and Electronics,

University of Science and Technology of China, Hefei 230026, China

Department of Modern Physics, University of Science and Technology of China, Hefei 230026, China

Abstract

As an important sequential work of the S-wave $B_c^{(*)}$ ($^1S_0(^3S_1)$) meson production at the large hadron electron collider (LHeC), we investigate the production of the P-wave excited B_c^{**} states (1P_1 and 3P_J with $J = 0, 1, 2$) via photoproduction mechanism within the framework of nonrelativistic QCD at the LHeC. Generally, the $e^- + P \rightarrow \gamma + g \rightarrow B_c^{**} + b + \bar{c}$ process is considered as the main production mechanism at an electron-proton collider due to the large luminosity of the gluon. However, according to our experience on the S-wave $B_c^{(*)}$ meson production at the LHeC, the extrinsic production mechanism, i.e., $e^- + P \rightarrow \gamma + c \rightarrow B_c^{**} + b$ and $e^- + P \rightarrow \gamma + \bar{b} \rightarrow B_c^{**} + \bar{c}$, could also provide dominating contributions at low p_T region. A careful treatment between these channels is performed and the results on total and differential cross sections, together with main uncertainties are discussed. Taking the quark masses $m_b = 4.90 \pm 0.40$ GeV and $m_c = 1.50 \pm 0.20$ GeV into account and summing up all the production channels, we expect to accumulate $(2.48^{+3.55}_{-1.75}) \times 10^4$ $B_c^{**}(^1P_1)$, $(1.14^{+1.49}_{-0.82}) \times 10^4$ $B_c^{**}(^3P_0)$, $(2.38^{+3.39}_{-1.74}) \times 10^4$ $B_c^{**}(^3P_1)$ and $(5.59^{+7.84}_{-3.93}) \times 10^4$ $B_c^{**}(^3P_2)$ events at the $\sqrt{S} = 1.30$ TeV LHeC in one operation year with luminosity $\mathcal{L} = 10^{33}$ cm $^{-2}$ s $^{-1}$. With such sizable events, it is worth studying the properties of excited P-wave B_c^{**} states at the LHeC.

*email: bihy@mail.ustc.edu.cn

I. INTRODUCTION

The doubly heavy meson physics has aroused great interest due to its nature, which can be studied in the framework of nonrelativistic QCD (NRQCD) [1]. The production of the doubly heavy meson can be factorized into a hard production of two heavy quark pairs which can be described by perturbation QCD (pQCD), and a soft term related to the nonperturbative binding of them. Thus, it is a good laboratory for testing NRQCD, pQCD and QCD potential models.

Among the doubly heavy mesons, the B_c meson¹ is especially interesting for its unique properties, which is the only observed meson composed of a heavy quark and a heavy antiquark of different flavors. Unlike the charmonium and bottomonium states, which have ‘hidden flavor’, the B_c meson is made of a charm quark and a bottom antiquark, and the production of B_c meson must be accompanied by additional heavy quarks especially in hadronic production [2, 3]. For example, production of a color-singlet $(c\bar{c})_1$ and a color-octet $(c\bar{c})_8$ quarkonium states are allowed for the channel $\gamma + g \rightarrow |(c\bar{c})_{1/8}\rangle + g/\gamma$. Therefore, compared with the production cross sections of hidden flavor quarkonia, the cross section of B_c meson is suppressed by not only the phase space but also the higher order in the coupling constants of leading-order diagrams. Due to the small production rate and the low colliding luminosity, the B_c meson was not found at LEP despite of careful searches [4–6]. At hadron colliders, the background is extremely serious. With much time and effort, the ground state B_c meson was finally observed by the CDF at Tevatron in 1998 [7, 8]. Now we also need more data to understand the properties of B_c meson, such as mass spectrum, lifetime and decay. Thus, the researches on various production mechanisms at high energy colliders are required to study the properties of B_c meson.

The hadronic production of B_c meson was amply studied directly via gluon-gluon fusion and etc, or indirectly via top quark, W or Higgs boson decays [9–31]. These studies indicated that at a hadron collider, such as the Large Hadron Collider (LHC) or Tevatron, sizable B_c events can be produced due to the powerful colliding energy and high luminosity. The B_c meson production at electron-positron colliders, such as super Z -factory and international linear collider were discussed in [32–39]. These lepton platforms have more clean background, hence

¹ S_0 B_c state is denoted as ground state B_c , 3S_1 B_c state is denoted as B_c^* , and four P-wave (1P_1 , 3P_0 , 3P_1 and 3P_2) B_c states are denoted as B_c^{**} .

are more suitable for precision measurement. For example, the authors in [32,33] are interested in the forward-backward asymmetry in the production of doubly heavy-flavored hadron at the Z -factory. The electron-proton collider, which combines the advantages of hadron collider and lepton collider, may provide good opportunity to study doubly heavy-flavored hadrons. Thus, we have studied the $B_c^{(*)}$ meson and doubly heavy baryon production [40,41] at the large hadron electron collider (LHeC) [42] and future circular collider-based electron-proton collider (FCC- ep), and we found these colliders are very helpful for study doubly heavy-flavored hadrons.

Recently, a new state has been observed by the ATLAS experiment [43], whose mass and decay mode are consistent with the theoretical prediction of the second S-wave state $B_c^\pm(2S)$. The B_c^\pm state is reconstructed through its decay to the ground state accompanied with two oppositely charged pions, and the B_c ground state is detected through its decay $B_c^\pm \rightarrow J/\psi\pi^\pm$. Besides, the excited B_c states can also decay (or in a cascade way) to the ground state through the electric or magnetic dipole transitions. In contrast with the hadronic decay, the feature of the electromagnetic decay of the excited B_c states is that the characteristic product is an additional photon with energy about dozens or hundreds of MeV [44–46] rather than pion. The measurements to the characteristic products, i.e., the pion or photon, can be treated as the signals for the discovery of the excited B_c states and the measurements of the ground or excited B_c states can provide the opportunity for extracting information on the mass spectrum of the ($c\bar{b}$) bound states and QCD potential models.

Generally speaking, the excited B_c states shall decay (or in a cascade way) to the ground state via electromagnetic or hadronic interactions with almost 100% probability, since B_c carry both b and c flavour-quantum number. Besides, its excited states may not be discriminated easily from its ground state in experiments [3]. Thus, it's necessary to estimate the production rate of excited P-wave B_c^{**} states, which will contribute to the production rate of S-wave $B_c^{(*)}$ states. On the other hand, it is helpful for the discovery of the excited B_c states to give the dynamic distributions of the production. Studies on the production of excited B_c states have been done in the literature [18, 19, 21, 32, 34, 38], and they found that the excited P-wave B_c^{**} states can provide about 14% \sim 17% contributions compared to the S-wave $B_c^{(*)}$ states.

As indicated in [40], large number of $B_c^{(*)}$ mesons (about 6×10^5 events per year) can be produced at LHeC. Motivated by the discovery of the second S-wave state B_c^\pm and the sizable $B_c^{(*)}$ events at the LHeC, we are interested in whether enough P-wave B_c^{**} events can be accumulated at the LHeC. In this paper, in addition to gluon-induced channel $\gamma+g \rightarrow B_c^{**}+b+\bar{c}$, two extrinsic heavy quark channels $\gamma+c \rightarrow B_c^{**}+b$ and $\gamma+\bar{b} \rightarrow B_c^{**}+\bar{c}$ are included. Although the density of \bar{b} and c quarks are small in proton, the contributions of $\gamma+c$ and $\gamma+\bar{b}$ channels cannot be neglected for the larger phase space and lower order in the coupling constants compared to the $\gamma+g$ channel.

The photoproduction of the B_c^{**} meson at the LHeC can be divided into three steps, which contain three subprocesses,

$$\begin{aligned}
e^- + P &\rightarrow \gamma + g \rightarrow (c\bar{b})[n] + b + \bar{c} \rightarrow B_c^{**} + b + \bar{c}, \\
e^- + P &\rightarrow \gamma + c \rightarrow (c\bar{b})[n] + b \rightarrow B_c^{**} + b, \\
e^- + P &\rightarrow \gamma + \bar{b} \rightarrow (c\bar{b})[n] + \bar{c} \rightarrow B_c^{**} + \bar{c}.
\end{aligned} \tag{1.1}$$

First, the photon beams are produced from the electron bremsstrahlung and the partons are radiated from the protons. The density of photon beams can be described by the Weizsäcker-Williams approximation (WWA) [47], and the parton densities are described by the parton distribution functions (PDFs). Second, photon beams interact with the partons and a diquark state with certain quantum numbers $(c\bar{b})[n]$ is produced, and this step can be calculated by the pQCD. Finally, the $(c\bar{b})[n]$ are bounded together to form the B_c^{**} meson through nonperturbative effect, which can be described by the nonperturbative matrix element, and the matrix element is proportional to the inclusive transition probability of the $(c\bar{b})[n]$ diquark to the bound state B_c^{**} . In this work, we only focus on four color-singlet diquark states of $(c\bar{b})[n]$, i.e., $(c\bar{b})_1[{}^1P_1]$, $(c\bar{b})_1[{}^3P_0]$, $(c\bar{b})_1[{}^3P_1]$, and $(c\bar{b})_1[{}^3P_2]^2$.

This paper is organized as follows: we present calculation details in Section II. The numerical results are given in Section III and the summary is presented in Section IV.

²We estimate the color-octet $|(c\bar{b})_8[{}^1S_0/{}^3S_1]g\rangle$ contribution to the P-wave B_c^{**} meson production and find this contribution is small (about 4% of the color-singlet contribution), thus we neglect it in the following discussion.

II. OUTLINE OF THE CALCULATION

Based on pQCD, the total cross section of the B_c^{**} meson production can be factorized into the convolution of the parton/photon density functions and the partonic cross section $d\hat{\sigma}_{\gamma i}(\mu, x_1, x_2)$ as follows:

$$d\sigma(e^- + P \rightarrow B_c^{**} + X) = \int dx_1 dx_2 \sum_{i=c,\bar{b},g} f_{\gamma/e^-}(x_1) f_{i/P}(\mu, x_2) d\hat{\sigma}_{\gamma i}(\mu, x_1, x_2), \quad (2.1)$$

here we have taken the renormalization scale μ_r and the factorization scale μ_f to be the same, i.e., $\mu_r = \mu_f = \mu$. $f_{i/P}$ are the PDFs and f_{γ/e^-} is the photon density function which is described by the WWA as

$$f_{\gamma/e^-}(x) = \frac{\alpha}{2\pi} \left[\frac{1 + (1-x)^2}{x} \ln \frac{Q_{\max}^2}{Q_{\min}^2} + 2m_e^2 x \left(\frac{1}{Q_{\max}^2} - \frac{1}{Q_{\min}^2} \right) \right], \quad (2.2)$$

where x is the fraction of the longitudinal momentum of the photon to electron beams. Q_{\min}^2 and Q_{\max}^2 are the minimum and maximum photon virtuality which can be expressed as

$$\begin{aligned} Q_{\min}^2 &= \frac{m_e^2 x^2}{1-x}, \\ Q_{\max}^2 &= (\theta_c E_e)^2 (1-x) + Q_{\min}^2, \end{aligned} \quad (2.3)$$

where θ_c is the electron-scattering angle and E_e is the the electron beam energy, which are determined by the collider. In this work we set $\theta_c = 32$ mrad which is consistent with the choices in Refs. [51, 52] and is satisfied with the requirement of $\theta_c \ll 1$ rad [53, 54].

To avoid the ‘double counting’ between $\gamma + g$ and $\gamma + q$ channels, the general-mass variable-flavor-number scheme (GM-VFNs) [55–59] is adopted here. The cross section under the GM-VFNs is

$$\begin{aligned} d\sigma(e^- + P \rightarrow B_c^{**} + X) &= f_{\gamma/e^-}(x_1) f_{g/P}(\mu, x_2) \otimes d\tilde{\sigma}_{\gamma g}(\mu, x_1, x_2) + \\ &\quad \sum_{q=c,\bar{b}} f_{\gamma/e^-}(x_1) [f_{q/P}(\mu, x_2) - f_{q/P}^{sub}(\mu, x_2)] \otimes d\tilde{\sigma}_{\gamma q}(\mu, x_1, x_2). \end{aligned} \quad (2.4)$$

$d\tilde{\sigma}_{\gamma g}$ contains mass logarithmic terms $\ln(Q^2/m_q^2)$, and these logarithmic terms originate in the Feynman diagrams which contains initial gluon splitting to a heavy quark pair $g \rightarrow q\bar{q}$. $d\sigma$ is the

infrared-safe partonic cross section which avoid the logarithmic terms through the subtraction of the term $f_{q/P}^{sub}(\mu, x_2)$:

$$f_{q/P}^{sub}(\mu, x_2) = \int_{x_2}^1 f_{g/P}(\frac{x_2}{y}) \frac{\alpha_s(\mu)}{2\pi} \ln \frac{\mu^2}{m_q^2} P_{g \rightarrow q}(y) \frac{dy}{y}, \quad (2.5)$$

where $P_{g \rightarrow q}(y) = \frac{1}{2}(1 - 2y + 2y^2)$ is the $g \rightarrow q\bar{q}$ splitting function.

The partonic hard cross section $d\tilde{\sigma}_{\gamma i}$ can also be factorized into a diquark production $(c\bar{b})[n]$ multiply by the nonperturbative matrix element $\langle \mathcal{O}^{B_c^{**}} \rangle$,

$$d\tilde{\sigma}_{\gamma i} = \frac{\langle \mathcal{O}^{B_c^{**}} \rangle}{4E_\gamma E_i |\vec{v}_\gamma - \vec{v}_i|} \overline{\sum} |\mathcal{M}|^2 d\Phi. \quad (2.6)$$

For the color-singlet B_c^{**} meson production, $\langle \mathcal{O}^{B_c^{**}} \rangle$ is related to the first derivative of the wave function at the origin of the $(c\bar{b})[n]$ bound state [1], i.e., $\langle \mathcal{O}^{B_c^{**}} \rangle \simeq |R'_P(0)|^2/(4\pi)$, and $R'_P(0)$ can be calculated from the potential model [48–50]. $d\Phi$ stands for the phase-space element and \mathcal{M} for the hard-scattering amplitudes of $(c\bar{b})[n]$ production which contains the precise spin and orbit information,

$$\mathcal{M}^{S=0, L=1} = \varepsilon_\alpha(p_3) \frac{d}{dq_\alpha} T|_{q=0}, \quad (2.7)$$

$$\mathcal{M}^{S=1, L=1} = \varepsilon_{\alpha\beta}^J(p_3) \frac{d}{dq_\alpha} T|_{q=0}. \quad (2.8)$$

where T is related to the Feynman diagrams and q is the relative momentum among the quarks inside $(c\bar{b})[n]$, which can be set as zero after the derivation of the amplitudes. $\varepsilon_\alpha(p_3)$ is the polarization vector of the angular momentum triplet 1P_1 diquark and $\varepsilon_{\alpha\beta}^J(p_3)$ stands for the polarization tensor of the spin-triplet P-wave 3P_J diquark. The summation over the polarizations obey the following relations:

$$\begin{aligned} \sum_{\text{polarizations}} \varepsilon_\alpha \varepsilon_{\alpha'}^* &= \Pi_{\alpha\alpha'}, \\ \varepsilon_{\alpha\beta}^0 \varepsilon_{\alpha'\beta'}^{0*} &= \frac{1}{3} \Pi_{\alpha\beta} \Pi_{\alpha'\beta'}, \\ \sum_{\text{polarizations}} \varepsilon_{\alpha\beta}^1 \varepsilon_{\alpha'\beta'}^{1*} &= \frac{1}{2} (\Pi_{\alpha\alpha'} \Pi_{\beta\beta'} - \Pi_{\alpha\beta'} \Pi_{\alpha'\beta}), \\ \sum_{\text{polarizations}} \varepsilon_{\alpha\beta}^2 \varepsilon_{\alpha'\beta'}^{2*} &= \frac{1}{2} (\Pi_{\alpha\alpha'} \Pi_{\beta\beta'} + \Pi_{\alpha\beta'} \Pi_{\alpha'\beta}) - \frac{1}{3} \Pi_{\alpha\beta} \Pi_{\alpha'\beta'}, \end{aligned} \quad (2.9)$$

where

$$\Pi_{\alpha\beta} = -g_{\alpha\beta} + \frac{p_{3\alpha} p_{3\beta}}{M^2}, \quad (2.10)$$

and M is the mass of B_c^{**} meson.

The Feynman diagrams and amplitudes are generated by FeynArts [60] and are provided in Appendix. Further simplification on the amplitudes are handled by FeynCalc [61] and FeynCalcFormLink [62]. Numerical calculations are performed by FormCalc [63].

III. NUMERICAL RESULTS

The derivative of the wave function at the origin $|R'_P(0)|^2 = 0.201 \text{ GeV}^5$ is taken from Ref. [48]. The P-wave B_c^{**} mesons mass M is taken as same with the S-wave $B_c^{(*)}$ mesons, which is the requirement for the NRQCD formalism and are explained in Ref. [19], i.e., $M = m_b + m_c$ with b -quark mass $m_b = 4.90 \text{ GeV}$ and c -quark mass $m_c = 1.50 \text{ GeV}$ [48]. The electron mass m_e is taken as $0.51 \times 10^{-3} \text{ GeV}$ and the fine-structure constant is chosen as $\alpha = 1/137$. The renormalization and factorization scale are set to be the transverse mass of the B_c^{**} meson $\mu = \mu_r = \mu_f = M_T = \sqrt{p_T^2 + M^2}$. We use CT10nlo [64] as default and the α_s is extracted from the PDFs.

The cross sections for all the production channels with four collision energies at two electron-proton colliders are presented in Table I, i.e., for the LHeC $\sqrt{S} = 1.30, 1.98 \text{ TeV}$ [42] which corresponds to two beam energy sets designs as $E_e = 60, 140 \text{ GeV}$ and $E_P = 7 \text{ TeV}$. For the FCC- ep we take $\sqrt{S} = 7.07, 10.00 \text{ TeV}$ [65] which correspond to two beam energy sets as $E_e = 250, 500 \text{ GeV}$ and $E_P = 50 \text{ TeV}$ separately. Here, we use $\sigma_{\gamma g}$, $\sigma_{\gamma c}$ and $\sigma_{\gamma \bar{b}}$ to denote the cross sections of $\gamma + g$, $\gamma + c$ and $\gamma + \bar{b}$ channels, respectively. Summing up all the contributions of three channels and four P-wave B_c^{**} states, we find that the contribution from P-wave B_c^{**} states can be 19.7%³, 19.9%, 19.8% and 20.2% of the S-wave $B_c^{(*)}$ state production (59.01, 95.91, 296.75 and 399.05 pb) [40] for above four colliding energies cases. That shows these ratios are larger than the corresponding ones at the Z -factory, LHC ($\sqrt{S} = 14 \text{ TeV}$) and Tevatron ($\sqrt{S} = 1.96 \text{ TeV}$), where the ratios are about 17.40%, 16.20% and 14.93%, respectively [19, 32]. We can conclude that the LHeC and FCC- ep colliding experiments might have advantages on the study of the P-wave B_c^{**} states, thus it is worth to study the excited states at these two

³Considering the main uncertainties from quark masses, this ratio should be $19.7_{-8.76}^{+6.82}\%$ at the LHeC with $\sqrt{S} = 1.30 \text{ TeV}$.

colliders. By summing up the four P-wave B_c^{**} states, We see also that the $\gamma + \bar{b}$ channel makes the largest contributions to the P-wave B_c^{**} state production, while the contributions from the $\gamma + g$ and $\gamma + c$ channels are at the same order which only provide about 5% and 1% to the total cross section for various electron-proton colliding energies. Besides, by summing up all the production channels, the four B_c^{**} states, i.e., 1P_1 , 3P_0 , 3P_1 and 3P_2 , provide individually about 21%, 10%, 20% and 48% contributions to the total cross section, respectively. The total cross section are similar at different colliding energies, and in the following, we focus on the B_c^{**} meson production at the $\sqrt{S} = 1.30$ TeV LHeC.

Table I: The cross sections (pb) for B_c^{**} production at two electron-proton colliders. Four electron-proton colliding energies are adopted, i.e., $\sqrt{S}=1.30$ and 1.98 TeV for LHeC, and $\sqrt{S}=7.07$ and 10.0 TeV for FCC- ep

	\sqrt{S}	$\sigma_{\gamma c}$				$\sigma_{\gamma \bar{b}}$				$\sigma_{\gamma g}$				Total
		1P_1	3P_0	3P_1	3P_2	1P_1	3P_0	3P_1	3P_2	1P_1	3P_0	3P_1	3P_2	
LHeC	1.30	4.87×10^{-2}	1.28×10^{-2}	2.68×10^{-2}	7.13×10^{-2}	2.30	1.10	2.27	5.22	1.27×10^{-1}	3.08×10^{-2}	7.72×10^{-2}	2.99×10^{-1}	11.6
	1.98	7.26×10^{-2}	1.94×10^{-2}	4.05×10^{-2}	1.07×10^{-1}	3.80	1.81	3.75	8.61	2.10×10^{-1}	5.06×10^{-2}	1.28×10^{-1}	4.90×10^{-1}	19.1
FCC- ep	7.07	1.68×10^{-1}	4.66×10^{-2}	9.64×10^{-2}	2.53×10^{-1}	11.8	5.55	11.6	26.7	6.34×10^{-1}	1.52×10^{-1}	3.93×10^{-1}	1.46	58.8
	10.0	2.14×10^{-1}	5.97×10^{-2}	1.23×10^{-1}	3.22×10^{-1}	16.3	7.63	15.9	36.7	8.65×10^{-1}	2.06×10^{-1}	5.35×10^{-1}	1.98	80.8

The B_c^{**} transverse momentum (p_T) distributions of all the production channels at the LHeC are shown in Figs.1(a,b). From the figures we can see that the contribution from $\gamma + \bar{b}$ channel dominates in the low p_T regions, but drops down more drastically than that from the $\gamma + g$ channel. Although the contribution of the $\gamma + g$ channel is suppressed in the low p_T region, it becomes the main contribution when the p_T goes up to large value range. We can see if one wants to select the P-wave B_c^{**} production signal from the $\gamma + g$ production channel at the LHeC, one can simply accept the events by imposing proper high lower p_T^{lower} cut ($p_T > p_T^{\text{lower}}$), and then the heavy quark initiated P-wave B_c^{**} production events can be suppressed. We find also from both Figs.1(a) and (b) that each differential cross section curve for the P-wave B_c^{**} meson from the $\gamma + \bar{b}$ production channel, has a pick around 1 GeV, which is quantitatively exceeded one or two order of the those for the $\gamma + g$ and $\gamma + c$ production channels. Thus, if the p_T acceptance range of the B_c^{**} mesons is limited all around 1 GeV, it is advantageous for the investigation of the P-wave B_c^{**} mesons from the $\gamma + \bar{b}$ production channel.

We present the rapidity (y) distributions of B_c^{**} mesons in Figs.2(a,b). There the asymmetry

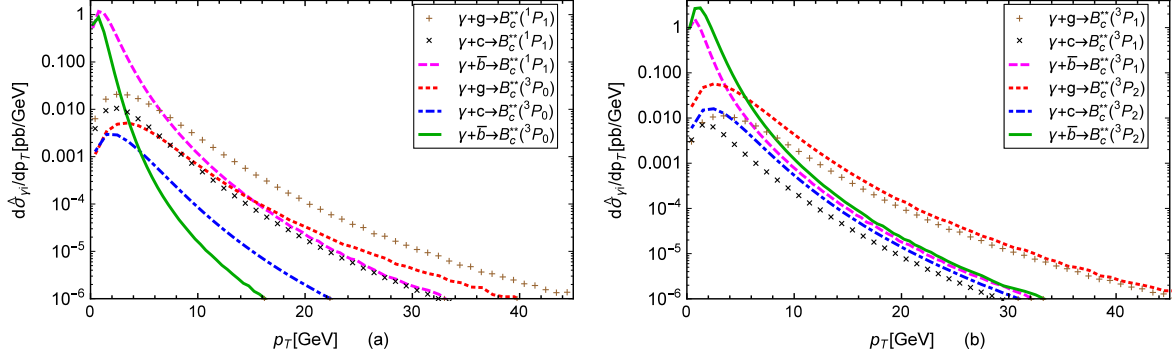


Figure 1: The transverse momentum distributions for the B_c^{**} meson at the $\sqrt{S} = 1.30$ TeV LHeC. (a) For the processes of $e^- + P \rightarrow \gamma + i \rightarrow B_c^{**}(^1P_1/^3P_0)$. (b) For the processes of $e^- + P \rightarrow \gamma + i \rightarrow B_c^{**}(^3P_1/^3P_2)$.

rapidity distributions indicate that the dominate contributions are located in the region around $y = 1$, due to the colliding energies of the incoming particles being not equal and the majority of the photons radiated from electron beams carrying less energies than the partons in the protons. Figs.2(a,b) show that the B_c^{**} meson rapidity distributions of all the three channels drop sharply when y increases from 2 to 3, while go down gently if y decreases from -4.

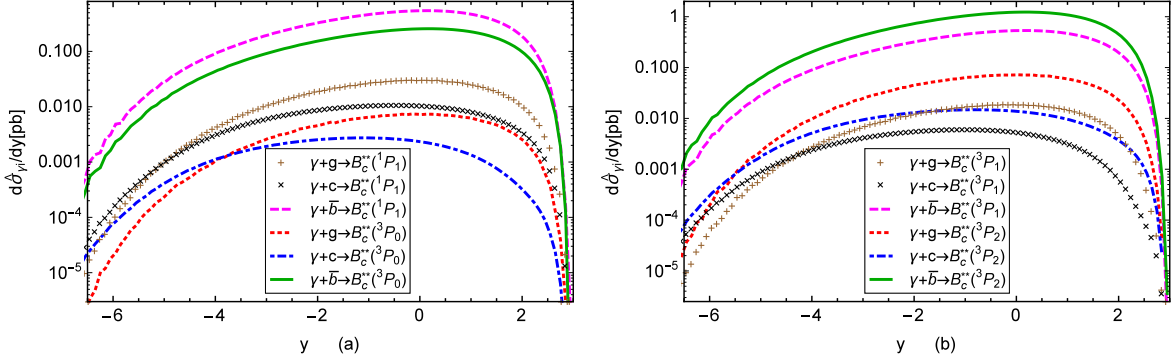


Figure 2: The rapidity distributions for the B_c^{**} meson at the $\sqrt{S} = 1.30$ TeV LHeC. (a) For the processes of $e^- + P \rightarrow \gamma + i \rightarrow B_c^{**}(^1P_1/^3P_0)$. (b) For the processes of $e^- + P \rightarrow \gamma + i \rightarrow B_c^{**}(^3P_1/^3P_2)$.

We know that the total cross section for B_c^{**} production should be sensitive to various experimental cuts, such as the p_T and y cuts on the final mesons. The cross sections by applying different p_T and y cuts on B_c^{**} mesons are presented in Table II and Table III separately. The data show that if the events are accepted with the condition of $p_T > 1.0$ GeV, the cross section via $\gamma + \bar{b}$ channel is about one order larger than that from the $\gamma + g$ channel, which can be

demonstrate also from the p_T distributions shown in Figs.1(a,b). By summing up the three channels and the four P-wave B_c^{**} states, we can get the ratio ($\frac{\sigma_{\text{cuts}}}{\sigma_{\text{No cuts}}}$) as 59.1%, 9.31%, 2.81% by applying p_T cuts as 1.0 GeV, 3.0 GeV and 5.0 GeV, respectively.

Table II: The cross sections (pb) for the B_c^{**} production at the $\sqrt{S} = 1.30$ TeV LHeC under various p_T cuts.

	$p_T \geq 1.0$ GeV				$p_T \geq 3.0$ GeV				$p_T \geq 5.0$ GeV			
	1P_1	3P_0	3P_1	3P_2	1P_1	3P_0	3P_1	3P_2	1P_1	3P_0	3P_1	3P_2
$\sigma_{\gamma c}$	4.49×10^{-2}	1.14×10^{-2}	2.37×10^{-2}	6.50×10^{-2}	2.60×10^{-2}	5.57×10^{-3}	1.10×10^{-2}	3.40×10^{-2}	1.16×10^{-2}	2.12×10^{-3}	4.38×10^{-3}	1.31×10^{-2}
$\sigma_{\gamma \bar{b}}$	1.44	3.43×10^{-1}	1.01	3.40	2.06×10^{-1}	9.10×10^{-3}	1.04×10^{-1}	3.51×10^{-1}	4.15×10^{-2}	8.52×10^{-4}	2.34×10^{-2}	5.34×10^{-2}
$\sigma_{\gamma g}$	1.21×10^{-1}	2.96×10^{-2}	7.41×10^{-2}	2.80×10^{-1}	8.31×10^{-2}	2.14×10^{-2}	5.54×10^{-2}	1.76×10^{-1}	4.56×10^{-2}	1.17×10^{-2}	3.37×10^{-2}	8.44×10^{-2}
Total	6.85				1.08				3.26×10^{-1}			

Table III: The cross sections (pb) for the B_c^{**} production at the $\sqrt{S} = 1.30$ TeV LHeC under various y cuts.

	$ y \leq 1.0$				$ y \leq 2.0$				$ y \leq 3.0$			
	1P_1	3P_0	3P_1	3P_2	1P_1	3P_0	3P_1	3P_2	1P_1	3P_0	3P_1	3P_2
$\sigma_{\gamma c}$	1.91×10^{-2}	4.47×10^{-3}	9.66×10^{-3}	2.65×10^{-2}	3.39×10^{-2}	7.93×10^{-3}	1.70×10^{-2}	4.72×10^{-2}	4.21×10^{-2}	1.03×10^{-2}	2.18×10^{-2}	6.00×10^{-2}
$\sigma_{\gamma \bar{b}}$	1.04	4.89×10^{-1}	1.02	2.34	1.78	8.44×10^{-1}	1.75	4.04	2.09	9.97×10^{-1}	2.07	4.75
$\sigma_{\gamma g}$	5.79×10^{-2}	1.40×10^{-2}	3.55×10^{-2}	1.37×10^{-1}	1.00×10^{-1}	2.41×10^{-2}	6.03×10^{-2}	2.34×10^{-1}	1.17×10^{-1}	2.84×10^{-2}	7.10×10^{-2}	2.76×10^{-1}
Total	5.19				8.94				10.5			

In photoproduction experiments, the study on inelastic B_c events can give information on the gluon distribution in the nucleon [66], and the inelasticity of the photoproduction can be denoted by the variable $z = \frac{p_{B_c} \cdot p_P}{p_\gamma \cdot p_P}$, where p_{B_c} , p_γ and p_P denote the four-momenta of the B_c , γ and proton, respectively. In the elastic domain, $z \approx 1$, and at low z region, the resolved effect (the hadronic components could be radiated from the photon) should also make some contributions [67]. Normally one can obtain clean samples of inelastic events in the range of $0.3 \lesssim z \lesssim 0.9$ [67–70]. Figs.3(a,b) show the distributions of variable z , and in Table IV we list the total cross sections at the $\sqrt{S} = 1.30$ TeV LHeC for different B_c^{**} production processes by accepting the events in the z range of $0.3 \leq z \leq 0.9$.

We present the results for $\mu = 0.75M_T$, M_T and $1.25M_T$ in Table V separately. For the $\gamma + c$ and $\gamma + g$ production channels, the cross sections decrease slightly when the scale becomes larger, while for the $\gamma + \bar{b}$ channels, the situation is opposite. At fixed order, the scale dependence of the prediction would lead to the uncertainties of final results. The scale uncertainties for the

Table IV: The cross section (pb) in the range of $0.3 \leq z \leq 0.9$ for different B_c^{**} production processes at the $\sqrt{S} = 1.30$ TeV LHeC.

	1P_1	3P_0	3P_1	3P_2	Total
$\sigma_{\gamma g}$	8.62×10^{-2}	2.15×10^{-2}	4.92×10^{-2}	1.99×10^{-1}	3.56×10^{-1}
$\sigma_{\gamma \bar{b}}$	1.39	6.80×10^{-1}	1.40	3.26	6.73
$\sigma_{\gamma c}$	3.34×10^{-2}	4.25×10^{-3}	1.01×10^{-2}	3.73×10^{-2}	8.51×10^{-2}

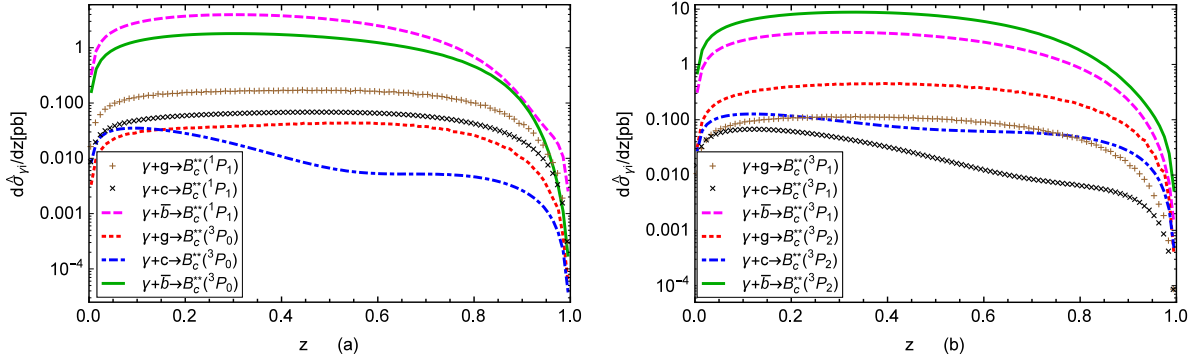


Figure 3: Differential cross sections $d\sigma/dz$ versus z for the B_c^{**} production at the $\sqrt{S} = 1.30$ TeV LHeC. (a) For the processes of $e^- + P \rightarrow \gamma + i \rightarrow B_c^{**}(^1P_1/^3P_0)$. (b) For the processes of $e^- + P \rightarrow \gamma + i \rightarrow B_c^{**}(^3P_1/^3P_2)$.

cross section (defined as $\frac{\sigma(\mu=\mu')-\sigma(\mu=M_T)}{\sigma(\mu=M_T)}$ with $\mu' = 0.75, 1.25M_T$) via the $\gamma + c$, $\gamma + \bar{b}$ and $\gamma + g$ channels are $-6\% \sim 8\%$, $-79\% \sim 31\%$ and $-11\% \sim 15\%$, respectively. By summing up all the three channels and the four P-wave B_c^{**} states, the total cross section still increases with the increasement of the scale owing to the large contributions from the $\gamma + \bar{b}$ channels. Such a large scale dependence could be reduced by involving higher-order QCD corrections. Furthermore, the renormalization scale dependence can be reduced by the QCD scale setting method [71, 72].

Table V: The cross sections (pb) for the B_c^{**} meson production at the $\sqrt{S} = 1.30$ TeV LHeC for $\mu = 0.75M_T$, M_T and $1.25M_T$ separately.

μ	$\sigma_{\gamma c}$				$\sigma_{\gamma \bar{b}}$				$\sigma_{\gamma g}$				Total
	1P_1	3P_0	3P_1	3P_2	1P_1	3P_0	3P_1	3P_2	1P_1	3P_0	3P_1	3P_2	
$0.75M_T$	5.27×10^{-2}	1.38×10^{-2}	2.89×10^{-2}	7.70×10^{-2}	5.15×10^{-1}	2.08×10^{-1}	4.67×10^{-1}	1.12	1.46×10^{-1}	3.54×10^{-2}	8.90×10^{-2}	3.44×10^{-1}	3.10
M_T	4.87×10^{-2}	1.28×10^{-2}	2.68×10^{-2}	7.13×10^{-2}	2.30	1.10	2.27	5.22	1.27×10^{-1}	3.08×10^{-2}	7.72×10^{-2}	2.99×10^{-1}	11.6
$1.25M_T$	4.56×10^{-2}	1.20×10^{-2}	2.52×10^{-2}	6.69×10^{-2}	2.99	1.45	2.99	6.80	1.14×10^{-1}	2.78×10^{-2}	6.93×10^{-2}	2.68×10^{-1}	14.9

Finally, we discuss the quark mass dependence of the cross sections. We take $m_c = 1.50 \pm$

0.20 GeV and $m_b = 4.90 \pm 0.40$ GeV into account. The m_c is fixed as its center values when discussing the uncertainty from $m_b = 4.90 \pm 0.40$ GeV and vice versa. The cross sections under different value of m_c and m_b are presented in Table VI and Table VII, respectively.

Table VI: The cross sections (pb) for B_c^{**} production by taking different value of m_c and fixing $m_b = 4.90$ GeV at the $\sqrt{S} = 1.30$ TeV LHeC.

m_c (GeV)	1.30	1.50	1.70
$\sigma_{\gamma c}({}^1P_1)$	6.33×10^{-2}	4.87×10^{-2}	3.80×10^{-2}
$\sigma_{\gamma c}({}^3P_0)$	1.52×10^{-2}	1.28×10^{-2}	1.08×10^{-2}
$\sigma_{\gamma c}({}^3P_1)$	3.44×10^{-2}	2.68×10^{-2}	2.12×10^{-2}
$\sigma_{\gamma c}({}^3P_2)$	9.58×10^{-2}	7.13×10^{-2}	5.42×10^{-2}
$\sigma_{\gamma \bar{b}}({}^1P_1)$	5.63	2.30	1.05
$\sigma_{\gamma \bar{b}}({}^3P_0)$	2.52	1.10	5.31×10^{-1}
$\sigma_{\gamma \bar{b}}({}^3P_1)$	5.48	2.27	1.05
$\sigma_{\gamma \bar{b}}({}^3P_2)$	12.5	5.22	2.43
$\sigma_{\gamma g}({}^1P_1)$	2.48×10^{-1}	1.27×10^{-1}	7.13×10^{-2}
$\sigma_{\gamma g}({}^3P_0)$	5.49×10^{-2}	3.08×10^{-2}	1.88×10^{-2}
$\sigma_{\gamma g}({}^3P_1)$	1.55×10^{-1}	7.72×10^{-2}	4.22×10^{-2}
$\sigma_{\gamma g}({}^3P_2)$	5.93×10^{-1}	2.99×10^{-1}	1.65×10^{-1}
Total	27.4	11.6	5.48

Table VII: The cross sections (pb) for B_c^{**} production by taking different value of m_b and fixing $m_c = 1.50$ GeV at the $\sqrt{S} = 1.30$ TeV LHeC.

m_b (GeV)	4.50	4.90	5.30
$\sigma_{\gamma c}({}^1P_1)$	7.39×10^{-2}	4.87×10^{-2}	3.33×10^{-2}
$\sigma_{\gamma c}({}^3P_0)$	2.05×10^{-2}	1.28×10^{-2}	8.29×10^{-3}
$\sigma_{\gamma c}({}^3P_1)$	4.12×10^{-2}	2.68×10^{-2}	1.81×10^{-2}
$\sigma_{\gamma c}({}^3P_2)$	1.07×10^{-1}	7.13×10^{-2}	4.95×10^{-2}
$\sigma_{\gamma \bar{b}}({}^1P_1)$	1.08	2.30	3.13
$\sigma_{\gamma \bar{b}}({}^3P_0)$	4.93×10^{-1}	1.10	1.47
$\sigma_{\gamma \bar{b}}({}^3P_1)$	1.03	2.27	3.10
$\sigma_{\gamma \bar{b}}({}^3P_2)$	2.46	5.22	7.04
$\sigma_{\gamma g}({}^1P_1)$	1.77×10^{-1}	1.27×10^{-1}	9.39×10^{-2}
$\sigma_{\gamma g}({}^3P_0)$	4.54×10^{-2}	3.08×10^{-2}	2.17×10^{-2}
$\sigma_{\gamma g}({}^3P_1)$	1.06×10^{-1}	7.72×10^{-2}	5.78×10^{-2}
$\sigma_{\gamma g}({}^3P_2)$	4.10×10^{-1}	2.99×10^{-1}	2.23×10^{-1}
Total	6.05	11.6	15.2

From the tables we can see that for most of the channels, the cross sections decrease when the c or b -quark mass becomes larger. The only exception is for the $\gamma + \bar{b}$ channel, whose cross

sections increase when the b -quark mass becomes larger. The cross sections are much more sensitive to m_c than to m_b , however, the $\gamma + \bar{b}$ channel provides most of the contributions, thus we conclude that the total cross section decreases when the c -quark mass becomes larger or the b -quark mass becomes smaller. Besides, it is clear that the cross sections of P-wave states are more sensitive to quark masses than the S-wave states as declared in [34, 38]. By summing up the cross sections of all production channels and their mass uncertainties, we obtain the total cross sections as

$$\sigma_{\text{LHeC}}^{\text{Total}} = 11.6_{-6.10}^{+15.9} \text{ pb, for } m_c = 1.50 \pm 0.20 \text{ GeV,} \quad (3.1)$$

$$\sigma_{\text{LHeC}}^{\text{Total}} = 11.6_{-5.53}^{+3.67} \text{ pb, for } m_b = 4.90 \pm 0.40 \text{ GeV,} \quad (3.2)$$

and by adding the errors from two mass uncertainties in quadrature, we finally obtain

$$\sigma_{\text{LHeC}}^{\text{Total}} = 11.6_{-8.24}^{+16.3} \text{ pb, for } m_b = 4.90 \pm 0.40 \text{ GeV and } m_c = 1.50 \pm 0.20 \text{ GeV.} \quad (3.3)$$

That means the contribution from total cross section of the P-wave B_c^{**} states can be about 11% \sim 27% of that from the S-wave $B_c^{(*)}$ state production ($59.0_{-28.3}^{+46.2}$ pb) [40] in the range of the uncertainties on heavy quark masses. So these excited state contributions should be taken into consideration, especially for the future high energy and high luminosity colliders.

With all the channels summed up, the shaded bands in Figs. 4, 5, 6 show the various uncertainties associated to the quark masses clearly. The central values correspond to $m_c = 1.50\text{GeV}$ and $m_b = 4.90\text{GeV}$, while the upper and lower bounds are obtained by setting $m_c = 1.30\text{GeV}$, $m_b = 5.30\text{GeV}$ and $m_c = 1.70\text{GeV}$, $m_b = 4.50\text{GeV}$, respectively.

IV. SUMMARY

In this paper, we studied the P-wave excited B_c^{**} (1P_1 and 3P_J with $J = 0, 1, 2$) meson photoproduction at the LHeC and three photoproduction channels, i.e., $e^- + P \rightarrow \gamma + g \rightarrow B_c^{**} + b + \bar{c}$, $e^- + P \rightarrow \gamma + c \rightarrow B_c^{**} + b$ and $e^- + P \rightarrow \gamma + \bar{b} \rightarrow B_c^{**} + \bar{c}$ are considered here. It is found that the production of the P-wave B_c^{**} states can contribute about 20% of the S-wave $B_c^{(*)}$ production at the LHeC and FCC- ep , if considering the fact that almost all of the P-wave B_c^{**} states decay to the ground state $B_c(^1S_0)$. Therefore, for the studying the production of B_c meson, the P-wave

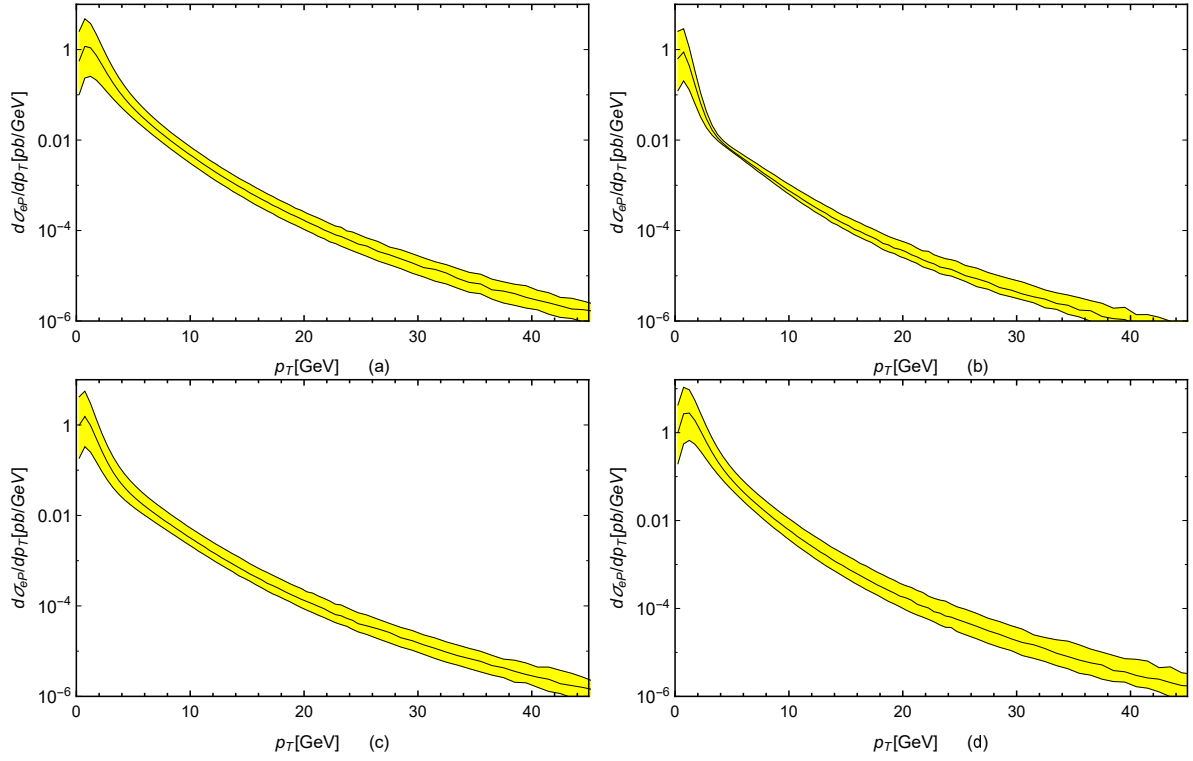


Figure 4: Uncertainties of the transverse momentum distributions from the quark masses for the B_c^{**} meson photoproduction at the $\sqrt{S} = 1.30$ TeV LHeC, where (a), (b), (c) and (d) denotes 1P_1 , 3P_0 , 3P_1 and 3P_2 B_c^{**} state, respectively.

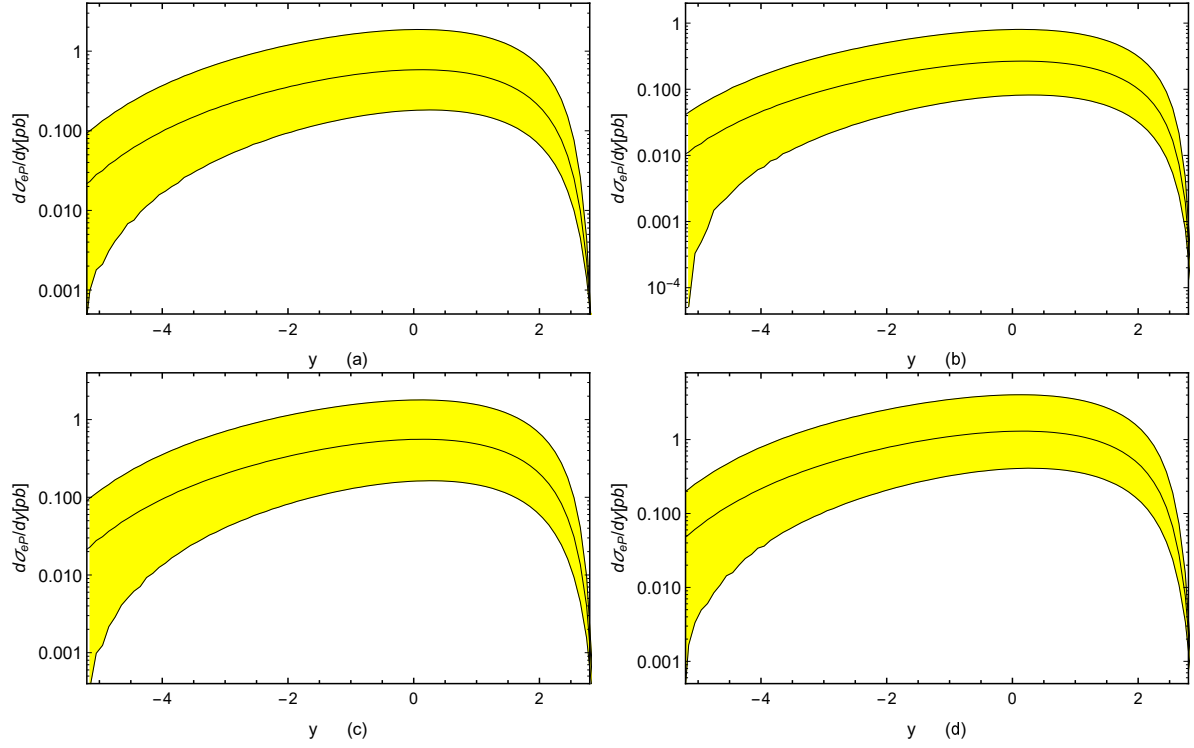


Figure 5: Uncertainties of the rapidity distributions from the quark masses for the B_c^{**} meson photoproduction at the $\sqrt{S} = 1.30$ TeV LHeC, where (a), (b), (c) and (d) denotes 1P_1 , 3P_0 , 3P_1 and 3P_2 B_c^{**} state, respectively.

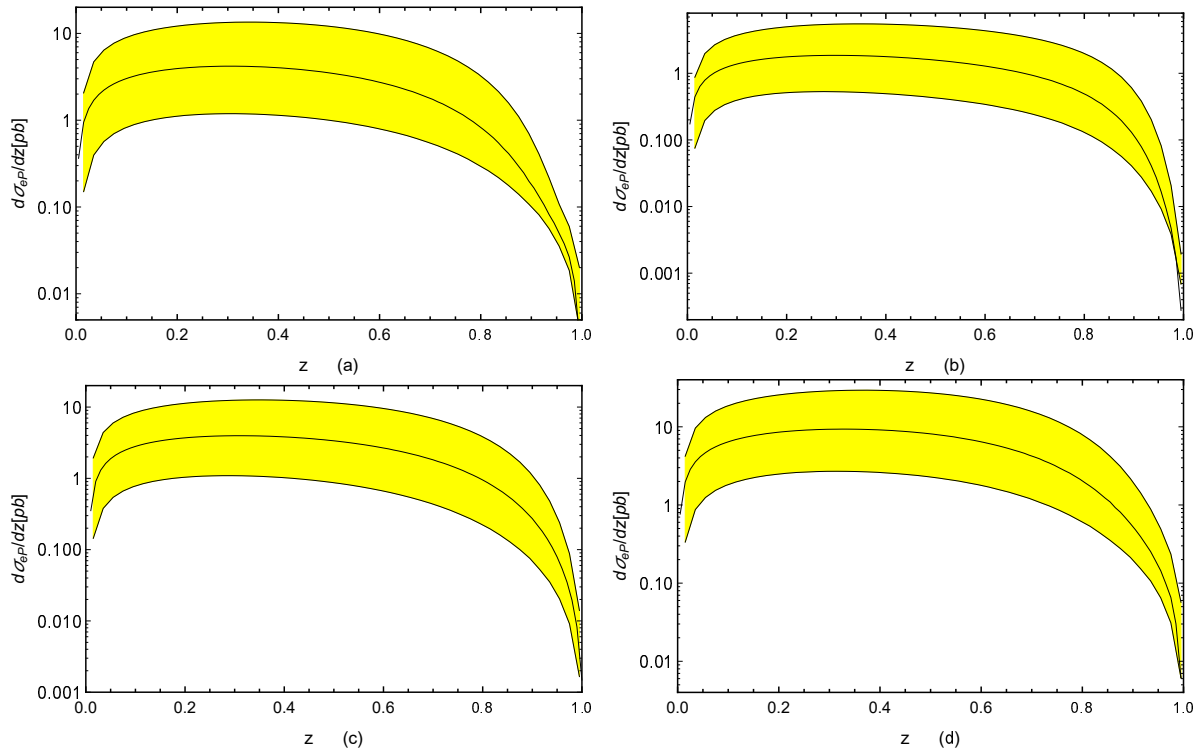


Figure 6: Uncertainties of the differential cross sections $d\sigma/dz$ versus z from the quark masses for the B_c^{**} meson photoproduction at the $\sqrt{S} = 1.30$ TeV LHeC, where (a), (b), (c) and (d) denotes 1P_1 , 3P_0 , 3P_1 and 3P_2 B_c^{**} state, respectively.

excited states should also be included. Taking the most prominent errors from the heavy quark masses, $m_b = 4.90 \pm 0.40$ GeV and $m_c = 1.50 \pm 0.20$ GeV, into account, we would expect to accumulate about $(2.48_{-1.75}^{+3.55}) \times 10^4 B_c^{**}(^1P_1)$, $(1.14_{-0.82}^{+1.49}) \times 10^4 B_c^{**}(^3P_0)$, $(2.38_{-1.74}^{+3.39}) \times 10^4 B_c^{**}(^3P_1)$ and $(5.59_{-3.93}^{+7.84}) \times 10^4 B_c^{**}(^3P_2)$ events at the LHeC in one operation year with $\sqrt{S} = 1.30$ TeV collision energy and the luminosity $\mathcal{L} = 10^{33}$ cm⁻²s⁻¹. We find that the dominant contributions come from low p_T region of $\gamma + \bar{b}$ channel, so it is possible to directly measure the P-wave B_c^{**} states at the LHeC and FCC- ep by using low p_T tagging technology, and thus is helpful to understand the mass spectrum of $(c\bar{b})$ bound states and to test the potential models.

Acknowledgments: This work is supported in part by the National Natural Science Foundation of China (No.11775211, No.11405173, No.11535002) and the CAS Center for Excellence in Particle Physics (CCEPP).

Appendix A: Feynman diagrams and hard-scattering amplitudes

We present the Feynman diagrams for $\gamma + g \rightarrow B_c^{**} + \bar{c} + b$ and $\gamma + c/\bar{b} \rightarrow B_c^{**} + b/\bar{c}$ in Figs.(7, 8). There are twenty-four hard-scattering amplitudes T_j ($T = \sum_{j=1}^{24} T_j$) for the subprocess $\gamma(p_1) + g(p_2) \rightarrow B_c^{**}(p_3) + \bar{c}(p_4) + b(p_5)$ which can be expressed as

$$\begin{aligned}
iT_1 &= ieg^3 Q_c \mathcal{C}_1 \bar{u}_{s'}(p_4) \gamma^\mu \frac{\Pi(p_3)}{(p_{32} + p_4)^2} \gamma^\mu \frac{\not{p}_3 + \not{p}_4 + m_c}{(p_3 + p_4)^2 - m_c^2} \not{\epsilon}(p_1) \frac{\not{p}_2 - \not{p}_5 + m_c}{(p_2 - p_5)^2 - m_c^2} \not{\epsilon}(p_2) v_s(p_5), \\
iT_2 &= ieg^3 Q_c \mathcal{C}_2 \bar{u}_{s'}(p_4) \gamma^\mu \frac{\Pi(p_3)}{(p_{32} + p_4)^2} \not{\epsilon}(p_1) \frac{\not{p}_{31} - \not{p}_1 + m_c}{(p_1 - p_{31})^2 - m_c^2} \gamma^\mu \frac{\not{p}_2 - \not{p}_5 + m_c^2}{(p_2 - p_5)^2 - m_c^2} \not{\epsilon}(p_2) v_s(p_5), \\
iT_3 &= ieg^3 Q_c \mathcal{C}_3 \bar{u}_{s'}(p_4) \gamma^\mu \frac{\Pi(p_3)}{(p_{32} + p_4)^2} \not{\epsilon}(p_1) \frac{\not{p}_{31} - \not{p}_1 + m_c}{(p_1 - p_{31})^2 - m_c^2} \not{\epsilon}(p_2) \frac{-\not{p}_{32} - \not{p}_4 - \not{p}_5 + m_c}{(p_{32} + p_4 + p_5)^2 - m_c^2} \gamma^\mu v_s(p_5), \\
iT_4 &= ieg^3 Q_c \mathcal{C}_4 \bar{u}_{s'}(p_4) \gamma^\mu \frac{\Pi(p_3)}{(p_{32} + p_4)^2} \gamma^\mu \frac{\not{p}_3 + \not{p}_4 + m_c}{(p_3 + p_4)^2 - m_c^2} \not{\epsilon}(p_2) \frac{\not{p}_1 - \not{p}_5 + m_c}{(p_1 - p_5)^2 - m_c^2} \not{\epsilon}(p_1) v_s(p_5), \\
iT_5 &= ieg^3 Q_c \mathcal{C}_5 \bar{u}_{s'}(p_4) \gamma^\mu \frac{\Pi(p_3)}{(p_{32} + p_4)^2} \not{\epsilon}(p_2) \frac{\not{p}_{31} - \not{p}_2 + m_c}{(p_2 - p_{31})^2 - m_c^2} \gamma^\mu \frac{\not{p}_1 - \not{p}_5 + m_c^2}{(p_1 - p_5)^2 - m_c^2} \not{\epsilon}(p_1) v_s(p_5), \\
iT_6 &= ieg^3 Q_c \mathcal{C}_6 \bar{u}_{s'}(p_4) \gamma^\mu \frac{\Pi(p_3)}{(p_{32} + p_4)^2} \not{\epsilon}(p_2) \frac{\not{p}_{31} - \not{p}_2 + m_c}{(p_2 - p_{31})^2 - m_c^2} \not{\epsilon}(p_1) \frac{-\not{p}_{32} - \not{p}_4 - \not{p}_5 + m_c}{(p_{32} + p_4 + p_5)^2 - m_c^2} \gamma^\mu v_s(p_5),
\end{aligned}$$

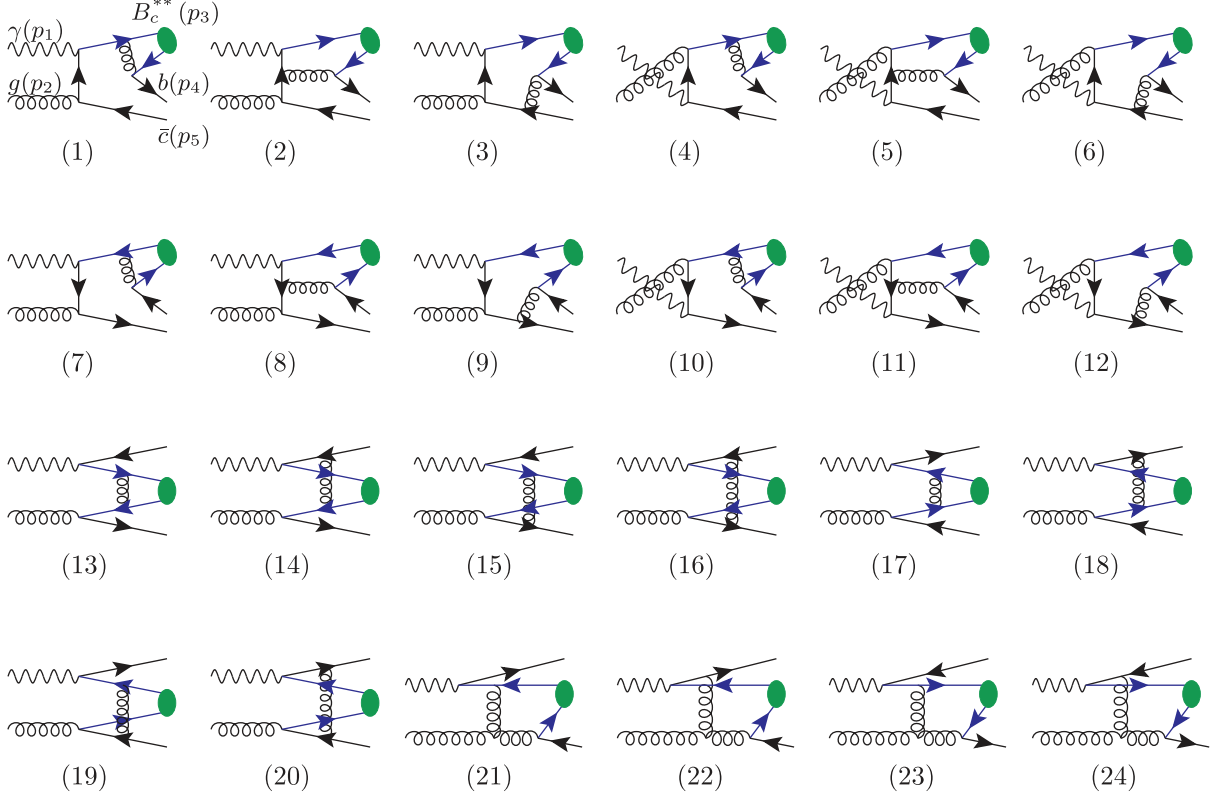


Figure 7: Feynman diagrams for the subprocess $\gamma + g \rightarrow B_c^{**} + b + \bar{c}$.

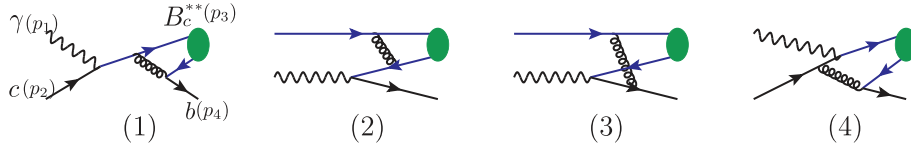


Figure 8: Feynman diagrams for the subprocess $\gamma + c \rightarrow B_c^{**} + b$. The Feynman diagrams for the subprocess $\gamma + \bar{b} \rightarrow B_c^{**} + \bar{c}$ can be obtained by the replacements $c \rightarrow \bar{b}$ and $b \rightarrow \bar{c}$.

$$\begin{aligned}
iT_7 &= ieg^3 Q_b \mathcal{C}_7 \bar{u}_{s'}(p_4) \not{\epsilon}(p_2) \frac{\not{p}_4 - \not{p}_2 + m_b}{(p_4 - p_2)^2 - m_b^2} \not{\epsilon}(p_1) \frac{-\not{p}_3 - \not{p}_5 + m_b}{(p_3 + p_5)^2 - m_b^2} \gamma^\mu \frac{\Pi(p_3)}{(p_{31} + p_5)^2} \gamma_\mu v_s(p_5), \\
iT_8 &= eg^3 Q_b \mathcal{C}_8 \bar{u}_{s'}(p_4) \not{\epsilon}(p_2) \frac{\not{p}_4 - \not{p}_2 + m_b}{(p_4 - p_2)^2 - m_b^2} \gamma^\mu \frac{\not{p}_1 - \not{p}_{32} + m_b}{(p_1 - p_{32})^2 - m_b^2} \not{\epsilon}(p_1) \frac{\Pi(p_3)}{(p_{31} + p_5)^2} \gamma_\mu v_s(p_5), \\
iT_9 &= ieg^3 Q_b \mathcal{C}_9 \bar{u}_{s'}(p_4) \gamma^\mu \frac{\not{p}_{31} + \not{p}_4 + \not{p}_5 + m_b}{(p_{31} + p_4 + p_5)^2 - m_b^2} \not{\epsilon}(p_2) \frac{\not{p}_1 - \not{p}_{32} + m_b}{(p_1 - p_{32})^2 - m_b^2} \not{\epsilon}(p_1) \frac{\Pi(p_3)}{(p_{31} + p_5)^2} \gamma_\mu v_s(p_5), \\
iT_{10} &= ieg^3 Q_b \mathcal{C}_{10} \bar{u}_{s'}(p_4) \not{\epsilon}(p_1) \frac{\not{p}_4 - \not{p}_1 + m_b}{(p_4 - p_1)^2 - m_b^2} \not{\epsilon}(p_2) \frac{-\not{p}_3 - \not{p}_5 + m_b}{(p_3 + p_5)^2 - m_b^2} \gamma^\mu \frac{\Pi(p_3)}{(p_{31} + p_5)^2} \gamma_\mu v_s(p_5), \\
iT_{11} &= ieg^3 Q_b \mathcal{C}_{11} \bar{u}_{s'}(p_4) \not{\epsilon}(p_1) \frac{\not{p}_4 - \not{p}_1 + m_b}{(p_4 - p_1)^2 - m_b^2} \gamma^\mu \frac{\not{p}_2 - \not{p}_{32} + m_b}{(p_2 - p_{32})^2 - m_b^2} \not{\epsilon}(p_2) \frac{\Pi(p_3)}{(p_{31} + p_5)^2} \gamma_\mu v_s(p_5), \\
iT_{12} &= ieg^3 Q_b \mathcal{C}_{12} \bar{u}_{s'}(p_4) \gamma^\mu \frac{\not{p}_{31} + \not{p}_4 + \not{p}_5 + m_b}{(p_{31} + p_4 + p_5)^2 - m_b^2} \not{\epsilon}(p_1) \frac{\not{p}_2 - \not{p}_{32} + m_b}{(p_2 - p_{32})^2 - m_b^2} \not{\epsilon}(p_2) \frac{\Pi(p_3)}{(p_{31} + p_5)^2} \gamma_\mu v_s(p_5),
\end{aligned}$$

$$\begin{aligned}
iT_{13} &= ieg^3 Q_c \mathcal{C}_{13} \bar{u}_{s'}(p_4) \not{\epsilon}(p_2) \frac{\not{p}_4 - \not{p}_2 + m_b^2}{(p_2 - p_4)^2 - m_b^2} \gamma^\mu \frac{\Pi(p_3)}{(p_1 - p_5 - p_{31})^2} \gamma^\mu \frac{\not{p}_1 - \not{p}_5 + m_c}{(p_1 - p_5)^2 - m_c^2} \not{\epsilon}(p_1) v_s(p_5), \\
iT_{14} &= ieg^3 Q_c \mathcal{C}_{14} \bar{u}_{s'}(p_4) \not{\epsilon}(p_2) \frac{\not{p}_4 - \not{p}_2 + m_b^2}{(p_2 - p_4)^2 - m_b^2} \gamma^\mu \frac{\Pi(p_3)}{(p_1 - p_5 - p_{31})^2} \not{\epsilon}(p_1) \frac{\not{p}_{31} - \not{p}_1 + m_c}{(p_1 - p_{31})^2 - m_c^2} \gamma^\mu v_s(p_5), \\
iT_{15} &= ieg^3 Q_c \mathcal{C}_{15} \bar{u}_{s'}(p_4) \gamma^\mu \frac{\not{p}_2 - \not{p}_{32} + m_b}{(p_2 - p_{32})^2 - m_b^2} \not{\epsilon}(p_2) \frac{\Pi(p_3)}{(p_1 - p_5 - p_{31})^2} \gamma^\mu \frac{\not{p}_1 - \not{p}_5 + m_c}{(p_1 - p_5)^2 - m_c^2} \not{\epsilon}(p_1) v_s(p_5), \\
iT_{16} &= ieg^3 Q_c \mathcal{C}_{16} \bar{u}_{s'}(p_4) \gamma^\mu \frac{\not{p}_2 - \not{p}_{32} + m_b}{(p_2 - p_{32})^2 - m_b^2} \not{\epsilon}(p_2) \frac{\Pi(p_3)}{(p_1 - p_5 - p_{31})^2} \not{\epsilon}(p_1) \frac{\not{p}_{31} - \not{p}_1 + m_c}{(p_1 - p_{31})^2 - m_c^2} \gamma^\mu v_s(p_5), \\
iT_{17} &= ieg^3 Q_b \mathcal{C}_{17} \bar{u}_{s'}(p_4) \not{\epsilon}(p_1) \frac{\not{p}_4 - \not{p}_1 + m_b^2}{(p_1 - p_4)^2 - m_b^2} \gamma^\mu \frac{\Pi(p_3)}{(p_2 - p_5 - p_{31})^2} \gamma^\mu \frac{\not{p}_2 - \not{p}_5 + m_c}{(p_2 - p_5)^2 - m_c^2} \not{\epsilon}(p_2) v_s(p_5), \\
iT_{18} &= ieg^3 Q_b \mathcal{C}_{18} \bar{u}_{s'}(p_4) \gamma^\mu \frac{\not{p}_1 - \not{p}_{32} + m_b}{(p_1 - p_{32})^2 - m_b^2} \not{\epsilon}(p_1) \frac{\Pi(p_3)}{(p_2 - p_5 - p_{31})^2} \gamma^\mu \frac{\not{p}_2 - \not{p}_5 + m_c}{(p_2 - p_5)^2 - m_c^2} \not{\epsilon}(p_2) v_s(p_5), \\
iT_{19} &= ieg^3 Q_b \mathcal{C}_{19} \bar{u}_{s'}(p_4) \not{\epsilon}(p_1) \frac{\not{p}_4 - \not{p}_1 + m_b^2}{(p_1 - p_4)^2 - m_b^2} \gamma^\mu \frac{\Pi(p_3)}{(p_2 - p_5 - p_{31})^2} \not{\epsilon}(p_2) \frac{\not{p}_{31} - \not{p}_2 + m_c}{(p_2 - p_{31})^2 - m_c^2} \gamma^\mu v_s(p_5), \\
iT_{20} &= ieg^3 Q_b \mathcal{C}_{20} \bar{u}_{s'}(p_4) \gamma^\mu \frac{\not{p}_1 - \not{p}_{32} + m_b}{(p_1 - p_{32})^2 - m_b^2} \not{\epsilon}(p_1) \frac{\Pi(p_3)}{(p_2 - p_5 - p_{31})^2} \not{\epsilon}(p_2) \frac{\not{p}_{31} - \not{p}_2 + m_c}{(p_2 - p_{31})^2 - m_c^2} \gamma^\mu v_s(p_5), \\
iT_{21} &= ieg^3 Q_b \mathcal{C}_{21} \bar{u}_{s'}(p_4) \not{\epsilon}(p_1) \frac{\not{p}_4 - \not{p}_1 + m_b}{(p_1 - p_4)^2 - m_b^2} \gamma^\rho \frac{\Pi(p_3)}{(p_{31} + p_5)^2 (p_{31} + p_5 - p_2)^2} \gamma^\nu \\
&\quad \cdot [g^{\mu\nu} (p_2 + p_5 + p_{31})^\rho + g^{\nu\rho} (p_2 - 2p_{31} - 2p_5)^\mu + g^{\rho\mu} (p_5 + p_{31} - 2p_2)^\nu] \epsilon_\mu v_s(p_5), \\
iT_{22} &= ieg^3 Q_b \mathcal{C}_{22} \bar{u}_{s'}(p_4) \gamma_\rho \frac{\not{p}_1 - \not{p}_{32} + m_b}{(p_1 - p_{32})^2 - m_b^2} \not{\epsilon}(p_1) \frac{\Pi(p_3)}{(p_{31} + p_5)^2 (p_{31} + p_5 - p_2)^2} \gamma^\nu \\
&\quad \cdot [g^{\mu\nu} (p_2 + p_5 + p_{31})^\rho + g^{\nu\rho} (p_2 - 2p_{31} - 2p_5)^\mu + g^{\rho\mu} (p_5 + p_{31} - 2p_2)^\nu] \epsilon_\mu v_s(p_5), \\
iT_{23} &= -ieg^3 Q_c \mathcal{C}_{23} \bar{u}_{s'}(p_4) \gamma_\nu \frac{\Pi(p_3)}{(p_{32} + p_4)^2 (p_{32} + p_4 - p_2)^2} \gamma^\rho \frac{\not{p}_1 - \not{p}_5 + m_c}{(p_1 - p_5)^2 - m_c^2} \not{\epsilon}(p_1) \\
&\quad \cdot [g^{\mu\nu} (p_2 + p_4 + p_{32})^\rho + g^{\nu\rho} (p_2 - 2p_4 - 2p_{32})^\mu + g^{\rho\mu} (p_4 + p_{32} - 2p_2)^\nu] \epsilon_\mu v_s(p_5), \\
iT_{24} &= -ieg^3 Q_c \mathcal{C}_{24} \bar{u}_{s'}(p_4) \gamma_\nu \frac{\Pi(p_3)}{(p_{32} + p_4)^2 (p_{32} + p_4 - p_2)^2} \not{\epsilon}(p_1) \frac{\not{p}_{31} - \not{p}_1 + m_c}{(p_1 - p_{31})^2 - m_c^2} \gamma^\rho \\
&\quad \cdot [g^{\mu\nu} (p_2 + p_4 + p_{32})^\rho + g^{\nu\rho} (p_2 - 2p_4 - 2p_{32})^\mu + g^{\rho\mu} (p_4 + p_{32} - 2p_2)^\nu] \epsilon_\mu v_s(p_5).
\end{aligned}$$

The four hard scattering amplitudes T_j ($T = \sum_{j=1}^4 T_j$) for the subprocess $\gamma(p_1) + c(p_2) \rightarrow B_c^{**}(p_3) + b(p_4)$ are

$$\begin{aligned}
iT_1 &= ieg^2 Q_c \mathcal{C}'_1 \bar{u}_{s'}(p_4) \gamma^\mu \frac{\Pi(p_3)}{(p_{32} + p_4)^2} \gamma^\mu \frac{\not{p}_3 + \not{p}_4 + m_c}{(p_3 + p_4)^2 - m_c^2} \not{\epsilon}(p_1) u_s(p_2), \\
iT_2 &= ieg^2 Q_b \mathcal{C}'_2 \bar{u}_{s'}(p_4) \not{\epsilon}(p_1) \frac{\not{p}_4 - \not{p}_1 + m_b}{(p_1 - p_4)^2 - m_b^2} \gamma^\mu \frac{\Pi(p_3)}{(p_2 - p_{31})^2} \gamma^\mu u_s(p_2), \\
iT_3 &= ieg^2 Q_b \mathcal{C}'_3 \bar{u}_{s'}(p_4) \gamma^\mu \frac{\not{p}_1 - \not{p}_{32} + m_b}{(p_1 - p_{32})^2 - m_b^2} \not{\epsilon}(p_1) \frac{\Pi(p_3)}{(p_2 - p_{31})^2} \gamma^\mu u_s(p_2), \\
iT_4 &= ieg^2 Q_c \mathcal{C}'_4 \bar{u}_{s'}(p_4) \gamma^\mu \frac{\Pi(p_3)}{(p_{32} + p_4)^2} \not{\epsilon}(p_1) \frac{\not{p}_2 - \not{p}_4 - \not{p}_{32} + m_c}{(p_2 - p_4 - p_{32})^2 - m_c^2} \gamma^\mu u_s(p_2),
\end{aligned}$$

and the amplitudes for the subprocess $\gamma(p_1) + \bar{b}(p_2) \rightarrow B_c^{**}(p_3) + \bar{c}(p_4)$ can be easily obtained from that of $\gamma(p_1) + c(p_2) \rightarrow B_c^{**}(p_3) + b(p_4)$. There $\Pi(p_3)$ stands for the spin-projection operator that depicts the $(c\bar{b})$ -pair evolving into the B_c^{**} meson

$$\Pi(p_3) = \sqrt{M} \left(\frac{\frac{m_b}{M} \not{p}_3 - \not{q} - m_b}{2m_b} \right) \Gamma \left(\frac{\frac{m_c}{M} \not{p}_3 + \not{q} + m_c}{2m_c} \right),$$

where $\Gamma = \gamma^5$ for the spin-singlet state, and $\Gamma = \gamma^\beta$ for the spin-triplet state. $\epsilon(p_1)$ and $\epsilon(p_2)$ are polarization vectors of the initial photon and gluon. p_{31} and p_{32} are four-momenta of the c -quark and \bar{b} -quark in the B_c^{**} meson, $p_{31} = \frac{m_c}{M}p_3 + q$ and $p_{32} = \frac{m_b}{M}p_3 - q$. The overall color factor \mathcal{C}_l and \mathcal{C}'_l are given by

$$\begin{aligned} \mathcal{C}_{l=(3,5,6,9,11,12,15,16,19,20)} &= \frac{1}{\sqrt{3}}(T^B T^A T^B)_{\alpha\beta}, \\ \mathcal{C}_{l=(1,2,4,7,8,10,13,14,17,18)} &= \frac{1}{\sqrt{3}}(T^A T^B T^B)_{\alpha\beta}, \\ \mathcal{C}_{l=(21,\dots,24)} &= \frac{i}{\sqrt{3}}f^{ABC}(T^B T^C)_{\alpha\beta}, \\ \mathcal{C}'_{l=(1,\dots,4)} &= \frac{1}{\sqrt{3}}C_F\delta_{\lambda\alpha}, \end{aligned}$$

where the factor $\frac{1}{\sqrt{3}}$ is due to the color-singlet nature of B_c^{**} meson. Superscript A stands for the color of the incident gluon, α and β are the color indices of the final outgoing b -quark and \bar{c} -quark, and λ is the color index of initial incoming c quark. $C_F = \frac{4}{3}$ is one of the Casimir operator eigenvalues of SU(3), f^{ABC} are the structure constants of SU(3) and $T^{A(B,C)}$ is the SU(3) generator in the fundamental representation. $Q_b = -\frac{1}{3}$ and $Q_c = \frac{2}{3}$ are electric charges of the b -quark and c -quark, respectively.

References

- [1] G. T. Bodwin, E. Braaten and G. P. Lepage, Phys. Rev. D **51**, 1125 (1995). Erratum: Phys. Rev. D **55**, 5853 (1997).
- [2] N. Brambilla *et al.* (Quarkonium Working Group), hep-ph/0412158.
- [3] N. Brambilla *et al.*, Eur. Phys. J. C **71**, 1534 (2011).
- [4] K. Ackerstaff *et al.* (OPAL Collaboration), Phys. Lett. B **420**, 157 (1998).

- [5] P. Abreu *et al.* (DELPHI Collaboration), Phys. Lett. B **398**, 207 (1997).
- [6] R. Barate *et al.* (ALEPH Collaboration), Phys. Lett. B **402**, 213 (1997).
- [7] F. Abe *et al.* (CDF Collaboration), Phys. Rev. Lett. **81**, 2432 (1998).
- [8] F. Abe *et al.* (CDF Collaboration), Phys. Rev. D **58**, 112004 (1998).
- [9] C. H. Chang and Y. Q. Chen, Phys. Rev. D **48**, 4086 (1993).
- [10] C. H. Chang, Y. Q. Chen, G. P. Han, and H. T. Jiang, Phys. Lett. B **364**, 78 (1995).
- [11] C. H. Chang, Y. Q. Chen, and R. J. Oakes, Phys. Rev. D **54**, 4344 (1996).
- [12] K. Kolodziej, A. Leike, and R. Ruckl, Phys. Lett. B **355**, 337 (1995).
- [13] E. Braaten, K. M. Cheung, and T. C. Yuan, Phys. Rev. D **48**, R5049 (1993).
- [14] A. V. Berezhnoy, A. K. Likhoded, and M. V. Shevlyagin, Phys. At. Nucl. **58**, 672 (1995).
- [15] A. V. Berezhnoy, V. V. Kiselev, A. K. Likhoded, and A. I. Onishchenko, Phys. At. Nucl. **60**, 1729 (1997).
- [16] S. P. Baranov, Phys. Rev. D **56**, 3046 (1997).
- [17] S. S. Gershtein, V. V. Kiselev, A. K. Likhoded, and A. V. Tkabladze, Phys. Usp. **38**, 1 (1995).
- [18] C. H. Chang, J. X. Wang, and X. G. Wu, Phys. Rev. D **77**, 014022 (2008).
- [19] C. H. Chang, J. X. Wang, and X. G. Wu, Phys. Rev. D **70**, 114019 (2004).
- [20] C. H. Chang and X. G. Wu, Eur. Phys. J. C **38**, 267 (2004).
- [21] C. H. Chang, C. F. Qiao, J. X. Wang, and X. G. Wu, Phys. Rev. D **71**, 074012 (2005).
- [22] X. G. Wu, Phys. Lett. B **671**, 318 (2009).
- [23] C. F. Qiao, L. P. Sun, D. S. Yang, and R. L. Zhu, Eur. Phys. J. C **71**, 1766 (2011).
- [24] Q. L. Liao, X. G. Wu, J. Jiang, Z. Yang, and Z. Y. Fang, Phys. Rev. D **85**, 014032 (2012).

- [25] C. H. Chang, C. Driouichi, P. Eerola, and X. G. Wu, *Comput. Phys. Commun.* **159**, 192 (2004).
- [26] C. H. Chang, J. X. Wang, and X. G. Wu, *Comput. Phys. Commun.* **174**, 241 (2006); *Comput. Phys. Commun.* **175**, 624 (2006).
- [27] X. Y. Wang and X. G. Wu, *Comput. Phys. Commun.* **183**, 442 (2012).
- [28] C. F. Qiao, C. S. Li, and K. T. Chao, *Phys. Rev. D* **54**, 5606 (1996).
- [29] K. M. Cheung, *Phys. Lett. B* **472**, 408 (2000).
- [30] C. H. Chang, C. F. Qiao, J. X. Wang, and X. G. Wu, *Phys. Rev. D* **72**, 114009 (2005).
- [31] J. Jiang and C. F. Qiao, *Phys. Rev. D* **93**, 054031 (2016).
- [32] X. C. Zheng, C. H. Chang, and Z. Pan, *Phys. Rev. D* **93**, 034019 (2016).
- [33] X. C. Zheng, C. H. Chang, T. F. Feng and Z. Pan, *Sci. China Phys. Mech. Astron.* **61**, no. 3, 031012 (2018).
- [34] Z. Yang, X. G. Wu, G. Chen, Q. L. Liao, and J. W. Zhang, *Phys. Rev. D* **85**, 094015 (2012).
- [35] Z. Yang, X. G. Wu, and X. Y. Wang, *Comput. Phys. Commun.* **184**, 2848 (2013).
- [36] J. Jiang, L. B. Chen, and C. F. Qiao, *Phys. Rev. D* **91**, 034033 (2015).
- [37] G. Chen, X. G. Wu, H. B. Fu, H. Y. Han, and Z. Sun, *Phys. Rev. D* **90**, 034004 (2014).
- [38] Z. Yang, X. G. Wu, L. C. Deng, J. W. Zhang and G. Chen, *Eur. Phys. J. C* **71**, 1563 (2011).
- [39] A. V. Berezhnoy, A. K. Likhoded, A. I. Onishchenko and S. V. Poslavsky, *Nucl. Phys. B* **915**, 224 (2017).
- [40] H. Y. Bi, R. Y. Zhang, H. Y. Han, Y. Jiang and X. G. Wu, *Phys. Rev. D* **95**, 034019 (2017).
- [41] H. Y. Bi, R. Y. Zhang, X. G. Wu, W. G. Ma, X. Z. Li and S. Owusu, *Phys. Rev. D* **95**, 074020 (2017).

- [42] J. L. Abelleira Fernandez *et al.* (LHeC Study Group), *J. Phys. G* **39**, 075001 (2012).
- [43] G. Aad *et al.* (ATLAS Collaboration), *Phys. Rev. Lett.* **113**, 212004 (2014).
- [44] T. Wang, Y. Jiang, W. L. Ju, H. Yuan and G. L. Wang, *JHEP* **1603**, 209 (2016).
- [45] A. P. Monteiro, M. Bhat and K. B. Vijaya Kumar, *Phys. Rev. D* **95**, 054016 (2017).
- [46] A. P. Monteiro, M. Bhat and K. B. Vijaya Kumar, *Int. J. Mod. Phys. A* **32**, 1750021 (2017).
- [47] S. Frixione, M. L. Mangano, P. Nason and G. Ridolfi, *Phys. Lett. B* **319**, 339 (1993).
- [48] E. J. Eichten and C. Quigg, *Phys. Rev. D* **49**, 5845 (1994).
- [49] E. J. Eichten and C. Quigg, *Phys. Rev. D* **52**, 1726 (1995).
- [50] W. Buchmuller and S. H. H. Tye, *Phys. Rev. D* **24**, 132 (1981).
- [51] C. F. Qiao and J. X. Wang, *Phys. Rev. D* **69**, 014015 (2004).
- [52] R. Li and K. T. Chao, *Phys. Rev. D* **79**, 114020 (2009).
- [53] M. Klasen, T. Kleinwort and G. Kramer, *Eur. Phys. J. direct* **1** (1998).
- [54] M. Klasen, *Rev. Mod. Phys.* **74**, 1221 (2002).
- [55] F. I. Olness, R. J. Scalise and W. K. Tung, *Phys. Rev. D* **59**, 014506 (1999).
- [56] M. A. G. Aivazis, F. I. Olness and W. K. Tung, *Phys. Rev. D* **50**, 3085 (1994).
- [57] M. A. G. Aivazis, J. C. Collins, F. I. Olness and W. K. Tung, *Phys. Rev. D* **50**, 3102 (1994).
- [58] J. Amundson, C. Schmidt, W. K. Tung and X. Wang, *JHEP* **0010**, 031 (2000).
- [59] B. A. Kniehl, G. Kramer, I. Schienbein and H. Spiesberger, *Eur. Phys. J. C* **41**, 199 (2005).
- [60] T. Hahn, *Comput. Phys. Commun.* **140**, 418 (2001).
- [61] V. Shtabovenko, R. Mertig and F. Orellana, *Comput. Phys. Commun.* **207**, 432 (2016).
- [62] F. Feng and R. Mertig, [arXiv:1212.3522](https://arxiv.org/abs/1212.3522).

- [63] T. Hahn and M. Perez-Victoria, *Comput. Phys. Commun.* **118**, 153 (1999).
- [64] A. Buckley, J. Ferrando, S. Lloyd, K. Nordström, B. Page, M. Rfenacht, M. Schnherr and G. Watt, *Eur. Phys. J. C* **75**, 132 (2015).
- [65] Y. C. Acar, A. N. Akay, S. Beser, H. Karadeniz, U. Kaya, B. B. Oner and S. Sultansoy, arXiv:1608.02190.
- [66] T. Ahmed *et al.* (H1 Collaboration), *Phys. Lett. B* **338**, 507 (1994).
- [67] C. Adloff *et al.* (H1 Collaboration), *Eur. Phys. J. C* **25**, 25 (2002).
- [68] M. Kramer, *Nucl. Phys. B***459**, 3 (1996).
- [69] C. Alexa *et al.* (H1 Collaboration), *Eur. Phys. J. C* **73**, 2466 (2013);
- [70] F. D. Aaron *et al.* (H1 Collaboration), *Eur. Phys. J. C* **68**, 401 (2010).
- [71] X. G. Wu, S. J. Brodsky and M. Mojaza, *Prog. Part. Nucl. Phys.* **72**, 44 (2013).
- [72] X. G. Wu, Y. Ma, S. Q. Wang, H. B. Fu, H. H. Ma, S. J. Brodsky and M. Mojaza, *Rept. Prog. Phys.* **78**, 126201 (2015).